THE FASEB JOURNAL • RESEARCH • www.fasebj.org

Controlling distinct signaling states in cultured cancer cells provides a new platform for drug discovery

Steven W. Poser,[*] Oliver Otto,[†] Carina Arps-Forker,[*] Yan Ge,[†,‡] Maik Herbig,[†] Cordula Andree,[§] Konrad Gruetzmann,[¶,‖] Melissa F. Adasme,[†] Szymon Stodolak,[#] Polyxeni Nikolakopoulou,[*] Deric M. Park,[,††] Alan Mcintyre,[#] Mathias Lesche,[†,‡‡] Andreas Dahl,[†,‡‡] Petra Lennig,[§§] Stefan R. Bornstein,[*,††] Evelin Schroeck,[¶,¶¶] Barbara Klink,[¶,¶¶] Ronen R. Leker,[‖‖] Marc Bickle,[§] George P. Chrousos,[##,***] Michael Schroeder,[†] Carlo Vittorio Cannistraci,[‡,†††] Jochen Guck,[†] and Andreas Androutsellis-Theotokis[*,#,††,‡‡,1]**

[*]Department of Internal Medicine III, [†]Biotechnology Center (BIOTEC), [‡]Biomedical Cybernetics Group, Department of Physics, Biotechnology Center (BIOTEC), Center for Molecular and Cellular Bioengineering (CMCB), Center for Systems Biology Dresden (CSBD), [§§]B CUBE - Center for Molecular Bioengineering, and [¶¶]Institute for Clinical Genetics, Faculty of Medicine Carl Gustav Carus, Technische Universität Dresden, Dresden, Germany; [§]Technology Development Studio, Max Planck Institute of Molecular Cell Biology and Genetics, Dresden, Germany; [¶]Core Unit for Molecular Tumor Diagnostics (CMTD), National Center for Tumor Diseases (NCT) Dresden, Dresden, Germany; German Cancer Consortium (DKTK), Dresden, Germany; [‖]German Cancer Research Center (DKFZ), Heidelberg, Germany; [#]Division of Cancer and Stem Cells, University of Nottingham, Nottingham, United Kingdom; [**]Department of Neurology, Committee on Clinical Pharmacology and Pharmacogenomics, The University of Chicago, Chicago, Illinois, USA; [††]Innate Repair, London, United Kingdom; [‡‡]Center for Regenerative Therapies Dresden, Dresden, Germany; [‖‖]Stroke Unit, Department of Neurology, Stroke Center and the Peritz and Chantal Sheinberg Cerebrovascular Research Laboratory, Hadassah-Hebrew University Medical Center, Jerusalem, Israel; [##]First Department of Pediatrics, National and Kapodistrian University of Athens Medical School, Athens, Greece; [***]Aghia Sophia Children's Hospital, Athens, Greece; and [†††]Brain Bio-Inspired Computing (BBC) Lab, IRCCS Centro Neurolesi Bonino Pulejo, Messina, Italy

ABSTRACT: Cancer cells can switch between signaling pathways to regulate growth under different conditions. In the tumor microenvironment, this likely helps them evade therapies that target specific pathways. We must identify all possible states and utilize them in drug screening programs. One such state is characterized by expression of the transcription factor Hairy and Enhancer of Split 3 (*HES3*) and sensitivity to *HES3* knockdown, and it can be modeled *in vitro*. Here, we cultured 3 primary human brain cancer cell lines under 3 different culture conditions that maintain low, medium, and high *HES3* expression and characterized gene regulation and mechanical phenotype in these states. We assessed gene expression regulation following *HES3* knockdown in the *HES3*-high conditions. We then employed a commonly used human brain tumor cell line to screen Food and Drug Administration (FDA)-approved compounds that specifically target the *HES3*-high state. We report that cells from multiple patients behave similarly when placed under distinct culture conditions. We identified 37 FDA-approved compounds that specifically kill cancer cells in the high-*HES3*–expression conditions. Our work reveals a novel signaling state in cancer, biomarkers, a strategy to identify treatments against it, and a set of putative drugs for potential repurposing.—Poser, S. W., Otto, O., Arps-Forker, C., Ge, Y., Herbig, M., Andree, C., Gruetzmann, K., Adasme, M. F., Stodolak, S., Nikolakopoulou, P., Park, D. M., Mcintyre, A., Lesche, M., Dahl, A., Lennig, P., Bornstein, S. R., Schroeck, E., Klink, B., Leker, R. R., Bickle, M., Chrousos, G. P., Schroeder, M., Cannistraci, C. V., Guck, J., Androutsellis-Theotokis, A. Controlling distinct signaling states in cultured cancer cells provides a new platform for drug discovery. FASEB J. 33, 000–000 (2019). www.fasebj.org

KEY WORDS: signal transduction · glioblastoma · brain tumor · glioma · drug repurposing

ABBREVIATIONS: bFGF, basic fibroblast growth factor; BindingDB, Binding Database; DAVID, Database for Annotation, Visualization and Integrated Discovery; DC, deformability cytometry; EGF, epidermal growth factor; FDA, Food and Drug Administration; FGFJI, basic fibroblast growth factor plus Janus kinase inhibitor; GO, Gene Ontology; *HES3*, Hairy and Enhancer of Split 3; iPS, induced pluripotent stem cell; JAK, Janus kinase; KEGG, Kyoto Encyclopedia of Genes and Genomes; MDR, multidrug resistant; PC, principal component; PCA, PC analysis; PPI, protein-protein interaction; RPMI, Roswell Park Memorial Institute; siRNA, small interfering RNA; STAT, signal transducer and activator of transcription

[1] Correspondence: Andreas Androutsellis-Theotokis, Haus 27 (DINZ), 1. OG, Zimmer 1.642, Medizinische Klinik und Poliklinik III und Zentrum für Innere Medizin, Universitätsklinikum Carl Gustav Carus an der TU Dresden, Fetscherstraße 74, 01307 Dresden, Germany. E-mail: andreas.theotokis@uniklinikum-dresden.de

doi: 10.1096/fj.201802603RR
This article includes supplemental data. Please visit *http://www.fasebj.org* to obtain this information.

Cancer cells cultured in different conditions are locked into different signal transduction states that render them sensitive to different properties. This plasticity likely helps cells evade therapy (1). Understanding as many of these states as possible will help us identify tailor-made treatments for each one. Here, we focus on such a state, characterized by expression of the transcription factor Hairy and Enhancer of Split 3 (*HES3*) (2) and sensitivity to *HES3* RNA interference (3).

The *HES3*+ state can be maintained in culture using established protocols that include an inhibitor of Janus kinase (JAK), a protein that opposes *HES3* expression (3, 4). The fact that JAK inhibition promotes cell growth in these conditions, whereas it opposes them in others (5, 6), stresses the importance of identifying and characterizing as many growth options as possible. Because *HES3*-expressing cells are found in tumor biopsies (3, 7) understanding this state is of clinical interest.

We used 3 primary cell lines, each derived from a different patient, cultured under 3 different monolayer conditions: *1*) common, serum-containing medium, characterized by high JAK activity and low *HES3* expression; *2*) serum-free medium containing the mitogen epidermal growth factor (EGF) that maintains cells in an intermediate *HES3* expression level (3) [this condition is oftentimes used for 3-dimensional glioblastoma cell culture systems (8)]; and *3*) serum-free medium containing the mitogen basic fibroblast growth factor (bFGF) and a JAK inhibitor, characterized by low JAK activity and high *HES3* expression levels (often used with monolayer primary neural stem cell cultures) (4). The cell culture medium compositions were designed to maintain cells locked into particular signaling states; they were not selected for the purpose of studying the effects of particular components of the medium (*e.g.*, the cytokines included in them).

We assessed gene expression and mechanical properties [by real-time deformability cytometry (DC)] in the different conditions and the response to *HES3* RNA interference in the conditions characterized by high *HES3* expression.

Finally, we switched to a human brain tumor cell line (U-87MG) that is commonly used in drug screening efforts to identify Food and Drug Administration (FDA)-approved compounds that are effective in the *HES3*-high state but not effective in the more commonly used serum-containing state, thus focusing our search on potentially overlooked putative therapeutics. We chose a widely used and easily available cell line for these experiments to help other scientists repeat and reproduce our data. At the same time, we were able to demonstrate that U-87MG cells can also be locked in different signaling states, further showcasing the robustness of our thesis.

We found distinct gene expression patterns associated with the 3 different culture conditions that were shared among all 3 patient-derived tumor cell lines. The mechanical assessment shows strong correlation between the *HES3*-high state and small cell size or increased deformability. Such mechanical properties have been observed in cells with metastatic competence and cancer stem cell properties and following dedifferentiation (9–12). Finally, we demonstrate, in a proof-of-concept manner using a library of 1600 FDA-approved compounds, that drug screening the same cell line under different conditions and, particularly, the *HES3*-high condition identifies new putative therapeutics for oncology.

MATERIALS AND METHODS

All methods were performed in accordance with the relevant guidelines and regulations. Gene expression data in cancerous tissues was obtained using the Human Protein Atlas (*http://www.proteinatlas.org*). Human figure schematics were generated using BioDigital (*http://www.biodigital.com*).

Cell culture

We used previously established human cell lines: U-87MG from American Type Culture Collection (ATCC; Manassas, VA, USA) and 3 primary human brain tumor cell lines (3, 13). For the primary lines, materials in excess of pathologic evaluation were used for research purposes in accordance with protocols approved by the Institutional Review Board of the U.S. National Institutes of Health (NIH; Bethesda, MD, US). Written consent had been obtained, and all research tumor tissues were deidentified. No animals were used in this work. All methods were performed in accordance with the relevant guidelines and regulations.

Three primary human brain tumor cell lines (X01, X04, and X08) were used in this work. X01 and X04 are from patients with glioblastoma multiforme, whereas X08 is from a patient with gliosarcoma (13, 14). The cell lines were previously established from acutely resected human tumor tissues. All human tissues in this study were obtained during surgical resections from patients with newly diagnosed or recurrent tumors. Materials in excess of pathological evaluation were used for research purposes in accordance with protocols approved by the Institutional Review Board of the NIH. Written consent was obtained, and all research tumor tissues were deidentified (3). Resected tissue was triturated in N2 medium containing 20 ng/ml EGF with a 1 ml pipette until no tissue clamps were seen; the triturate was allowed to settle for 1 min, and the supernatant was collected, diluted in N2 containing EGF, and plated. Cells were expanded in serum-free DMEM and F12 medium (10-090-CV; Mediatech, Manassas, VA, USA) with N2 supplement and EGF (20 ng/ml; R&D Systems, Minneapolis, MN, USA) for 5 d under 5% oxygen conditions and were replated fresh or from frozen stocks at 1000–10,000 cells/cm^2. This was repeated for several passages. For the experiments, frozen stocks were thawed and expanded as previously described, and, upon passaging, they were replated into different culture conditions, as described in the Results section. Gene expression and mechanical analysis were performed after 5 d in culture. For a complete protocol, see Poser *et al.* (15).

We also used the human brain tumor cell line U-87MG [HTB-14; American Type Culture Collection (ATCC)]. This was propagated in serum-containing Roswell Park Memorial Institute (RPMI) medium. It was then replated in different medium according to experimental needs, as described in the Results.

Gene expression profiling by RNA sequencing

RNA was extracted using the High Pure RNA Isolation Kit (Roche, Basel, Switzerland), and samples were subjected to the standard workflow for strand-specific RNA sequencing library preparation (Ultra Directional RNA Library Prep; NEB, Ipswich, MA, USA). Libraries were equimolar, pooled, and sequenced on an Illumina (San Diego, CA, USA) HiSeq 2500, resulting in about 26–35 million single-end reads per library. After sequencing, FastQC (*http://www.bioinformatics.babraham.ac.uk/*) was used to

perform a basic quality control on the resulting reads. As an additional control, library diversity was assessed by redundancy investigation in the reads. Reads were aligned to the human reference (GRCh38) using GSNAP (v.2014-12-17) (16), and Ensembl (*http://dec2014.archive.ensembl.org/index.html*) gene annotation v.78 was used to detect splice sites. The uniquely aligned reads were counted with featureCounts (v.1.4.6) (17) and the same Ensembl annotation. Normalization of the raw read counts based on the library size and testing for differential expression between conditions was performed with the DESeq2 R package (v.1.6.2) (18). Experiments addressing the effect of cell culture medium composition were performed in triplicates; effects addressing the effect of *HES3* RNA interference were performed in quadruplicates.

Systems biomedical analysis (experiments under different culture conditions)

For the RNA sequencing data analysis, we performed principal component (PC) analysis (PCA) to investigate the presence of gene expression patterns related with the experimental culture conditions and the cell lines in a nonbiased (unsupervised) manner (19). PCA is an unsupervised machine learning method, by which original multiple variables (here, genes) are converted into a set of linearly uncorrelated orthogonal variables (PCs) in such a way that the first PC (PC1) accounts for the largest variability of the data, and the succeeding PCs account for the variance in decreasing order under the constraint that each component is orthogonal to the preceding ones (20).

For the heat map generation, PC1 loadings were normalized according to the maximum absolute value to −1 and 1. The top 1% most significantly regulated genes (the list of which is reported in Supplemental Table S1) were selected for further analysis. For the *x* axis, samples were ordered from X01, X04, and X08 for each culture condition. For the *y* axis, the genes were ordered according to an unsupervised machine learning technique, minimum curvilinear embedding (MCE), by using the Euclidean distance (19, 21). The color bar indicates the expression as the log10 (1+ raw expression read counts). The name of the ordered genes from 1 to 400 are presented in Supplemental Table S1.

Mechanomics network

To determine the main functions related to the top 1% most significantly regulated genes, we performed functional annotation analysis in Database for Annotation, Visualization and Integrated Discovery (DAVID; *https://david.ncifcrf.gov/*) (22, 23) using Ensemble geneID. Then, we considered all the significant Gene Ontology (GO) terms and Kyoto Encyclopedia of Genes and Genomes (KEGG; *https://www.genome.jp/kegg/*) pathways that achieved a Benjamini-corrected *P* value lower than 0.05 (Supplemental Table S2). Because the highest significant GO term (GO:0008092 ~ cytoskeletal protein binding) and the highest significant pathway (hsa04510: focal adhesion) were related to cell mechanics, we decided to further investigate the list of genes contained in the top 20 significant cell mechanics–related GO annotations. To this aim, we proceeded to the construction of a mechanomic protein-protein interaction (PPI) network in which only those genes belonging to the top 20 significant cell mechanics–related GO annotations were considered (201 unique genes were retrieved from the original list of the top 1% regulated genes that were 400). Nearly half of the top 1% most significantly regulated genes are involved with cell mechanics. The Search Tool for the Retrieval of Interacting Genes/Proteins (*https://string-db.org/*) was used to build the PPI network (24). To select reliable interactions, only links validated by experimental evidence and higher than a 0.7 cutoff were considered to build the network. For visualization purposes, we used the Cytoscape software (25). The bigger the node size, the more interactions the node has. Green-filled gene names are significantly differently expressed between EGF and basic fibroblast growth factor plus Janus kinase inhibitor (FGFJI), and their interaction is indicated by thick green lines. The interaction between a green node and a gray node is indicated by thicker lines than the interaction between gray nodes to highlight the potential functional interactions of these significant green-node genes. Round rectangle with blue boundary genes are cell surface markers, whereas diamond shapes with red boundary nodes are transcription factors. According to the top 20 significant cell mechanics–related functional annotations, the nodes belonging to the most significant GO term and the most significant KEGG terms are identified by means of a dashed-line rectangle; genes not included in the respective rectangles are identified with a star symbol of the same rectangle color. Some genes belonging to the dashed-line rectangles also belong to the modules at the center of the image. These genes are indicated only in the modules to avoid repetition in the image. These genes are indicated with a start whose color matches the dashed rectangle they also belong to. Another 3 genes belonging to the pin rectangle are also associated with the ubiquitin C gene, and these are marked by a pink star and are only placed around ubiquitin C. Core functional subnetwork modules differentially activated between FGFJI and EGF were identified, and the elements (genes) of each module were characterized according to their top functional annotation term in the top 20 list using different symbols. To reflect the difference of each module between the FGFJI and EGF, the average expression by considering the whole included genes in each module were represented with a bar plot beside the module. To correct for the magnitude discrepancy of each gene (forcing an equal contribution of every gene to the final pattern), the expression of every gene is, first, normalized by dividing the sum of this gene's expression in FGFJI or EGF in the investigated module, and then all the composed genes of this module in FGFJI or EGF state are averaged to get the general expression of the particular state.

Pathway analysis (cell culture condition experiments)

Pathway analysis was done using 2 different methods. First, GO term and KEGG pathway enrichment of differentially expressed genes (adjusted $P < 0.05$) were calculated using DAVID Bioinformatics Resource (22) based on Ensembl IDs. The background set consisted of all genes passed to DESeq2. Second, the R package fgsea (*https://github.com/ctlab/fgsea*) was used for a full gene set enrichment analysis based on all genes; –log10(*P* value) × log2(fold-change) was used as rank function, and 100,000 permutations were done for enrichment *P* value calculation. KEGG pathways were plotted using the R package pathview (26).

Comparison of growth medium experiment with *HES3* small interfering RNA knockdown experiment

Raw gene read counts of all samples were regularized logarithmic transformed using DESeq2 R package (18). Samples were clustered using Spearman rank correlation, Pearson correlation, and Euclidean distance based on transformed counts of all genes. Cluster heat maps were drawn using the ComplexHeatmap R package (27).

Real-time DC

Real-time DC was performed as previously described (28, 29). Briefly, it allows a marker-free, continuous cell mechanical characterization of large cell populations with analysis rates

>100 cells/s. Cells are flowed through a microfluidic channel constriction and deformed without contact by shear stresses and pressure gradients. Cell size and deformation is extracted from the high-speed camera images in real time and can be transformed into an elastic modulus (of stiffness of a cell) by applying an analytical model relating geometrical parameters to material properties (29). Statistical data analysis was carried out utilizing mixed models (30, 31) by assuming random as well as fixed effects for the experimental repeats.

HES3 small interfering RNA transfection of X0 glioblastoma cells

Cells were plated into 6-well plates containing N2 medium supplemented with 20 ng/ml FGF and 200 nM Jak inhibitor (FGFJI). Forty hours later, cells were transfected with either scrambled control small interfering RNA (siRNA) (SC37007; Santa Cruz Biotechnology, Dallas, TX, USA) or *HES3* siRNA (SC88003; Santa Cruz Biotechnology) using Lipofectamine RNAiMax (Thermo Fisher Scientific, Waltham, MA, USA) transfection reagent as described by the manufacturer. Cells were collected 24 h post-transfection, and total RNA was isolated using a HighPure RNA Isolation Kit (Roche). Experiments were performed in quadruplicates for each cell line and siRNA transfection. RNA quality was assessed using an Agilent 2100 Bioanalyzer (Agilent Technologies, Santa Clara, CA, USA).

Drug screening

White Corning 384-well plates (3570) were coated with 40 μl of 4950 μg/ml polyornithine (P-365; MilliporeSigma, Burlington, MA, USA) at 37°C overnight. The next day, the plates were washed 5 times with water using a BioTek (Winooski, VT, USA) EL 406 plate washer. The plates were then coated with 40 μl of 1 mg/ml fibronectin (1030-Fn; R&D Systems) for 2 h at 37°C and then washed 2 times with PBS. Either 15 or 50 nl of either 10 mM library compounds (MicroSource Pharmakon library; Microsource Discovery Systems, Gaylordsville, CT, USA) or 100% DMSO as negative control or 1 mM Staurosporine (ACROS 328532500) were dispensed with a Labcyte (San Jose, CA, USA) Echo 550 to screen the library at 3 and 10 μM, respectively. U87 cells were seeded in the plates with a WellMate drop dispenser (Thermo Fisher Scientific) at a density of 3000 cells per well in 50 μl N2 medium and incubated for 20 h at 37°C in 5% CO_2. Cell viability was assayed using Perkin Elmer (Waltham, MA, USA) ATPLite (6016731) according to vendor's instructions. For the dose-dependent verification assay, cells were seeded in N2 medium with or without serum to test the specificity of compound action. The 6 compounds that were selected for the dose curve experiment were Ebselen (ab142424; Abcam, Cambridge, MA, USA), Ramelteon (S1259; Selleckchem, Houston, TX, USA), Raloxifene HCl (S1227; Selleckchem), Triclosan (S4541; Selleckchem), Clioquinol (S4601; Selleckchem), and Miconazole Nitrate (S1956; Selleckchem).

Computational analysis of selected compounds

Compound structures were downloaded from PubChem (*https://pubchem.ncbi.nlm.nih.gov/*) on August 7, 2017, in spatial data file format and compared using the Score Matrix Service with standard settings of 2D Tanimoto similarity. The heat map was generated with the Heatplus package v.2.8.0 in R 3.0.2 with hierarchical clustering over average distances. Drug targets were retrieved from Binding Database (BindingDB; *https://www.bindingdb.org/bind/index.jsp*), drug disease relations from Therapeutic Target Database (TTD; *https://db.idrblab.org/ttd/*), and protein structures from Protein Data Bank (PDB; *https://www.rcsb.org/*). The corresponding drug-target-disease networks were visualized with Cytoscape v.3.5.1. The drug-target network shows only targets with 2 or more compounds.

RESULTS

Prior to the treatments described, the primary cell lines used here had never been exposed to serum or other undefined culture medium supplements. Their tumorigenic potential was previously established (13). For standard expansion and passaging, cell lines were cultured in monolayer form in the presence of EGF (**Fig. 1*A***) based on previously published methods (3, 15). Each cell line was split into separate flasks and cultured in 3 distinct conditions for 5 d, containing either 10% fetal bovine serum (Serum), EGF, or bFGF including a JAK inhibitor (bFGF+JAK Inhibitor = FGFJI), all in a 5% oxygen incubator. The 3 conditions maintain the cells under different signal transduction states, all of which allow for efficient growth (3). Serum contains many strong activators of the JAK–signal transducer and activator of transcription (STAT) signaling pathway that oppose *HES3* expression (4). EGF is a relatively mild activator of the JAK-STAT pathway and maintains these cells in a state of intermediate *HES3* expression; FGFJI suppresses the JAK-STAT pathway and strongly promotes *HES3* expression. Following culture under each specific condition, cells were collected for RNA sequencing (32) or real-time DC (28).

Gene expression regulation under different culture conditions

We performed a PCA and found that PC1 is related to culture condition and PC2 is related to the cell line (each cell line is derived from a different patient) (Fig. 1*B*). The data show an undisputable group discrimination (evident linear separations) based on PC1, suggesting that all 3 cell lines respond similarly in terms of gene expression when placed under each culture condition. The Serum culture condition is separated from the other 2 conditions by a larger margin (support vector machine maximum margin computation values, FGFJI to EGF: 0.2; EFG to Serum: 1.0) (33). A heat map generated from the top ~1% discriminative genes (top 400 genes that represent the top ~1% of genes with the highest absolute PC1 loading values) is presented in Fig. 1*C*. The list of genes is in Supplemental Table S1.

The GO enrichment analysis of these genes revealed that both the most significant GO term (GO:0008092 ~ cytoskeletal protein binding, corrected $P < 0.0001$) and the most significant pathway (hsa04510:Focal adhesion, corrected $P < 0.0001$) are related to cell mechanics (Supplemental Table S2).

For the GO term analysis, the 400 top genes were used for DAVID annotation analysis (using Ensemble geneID). We focused on mechanics-related GO terms, which were sorted by Benjamini multiple correction; the top 20 GO terms were chosen for further network construction. For the network construction, the genes belonging to mechanics-related GO terms from the list of 400 genes

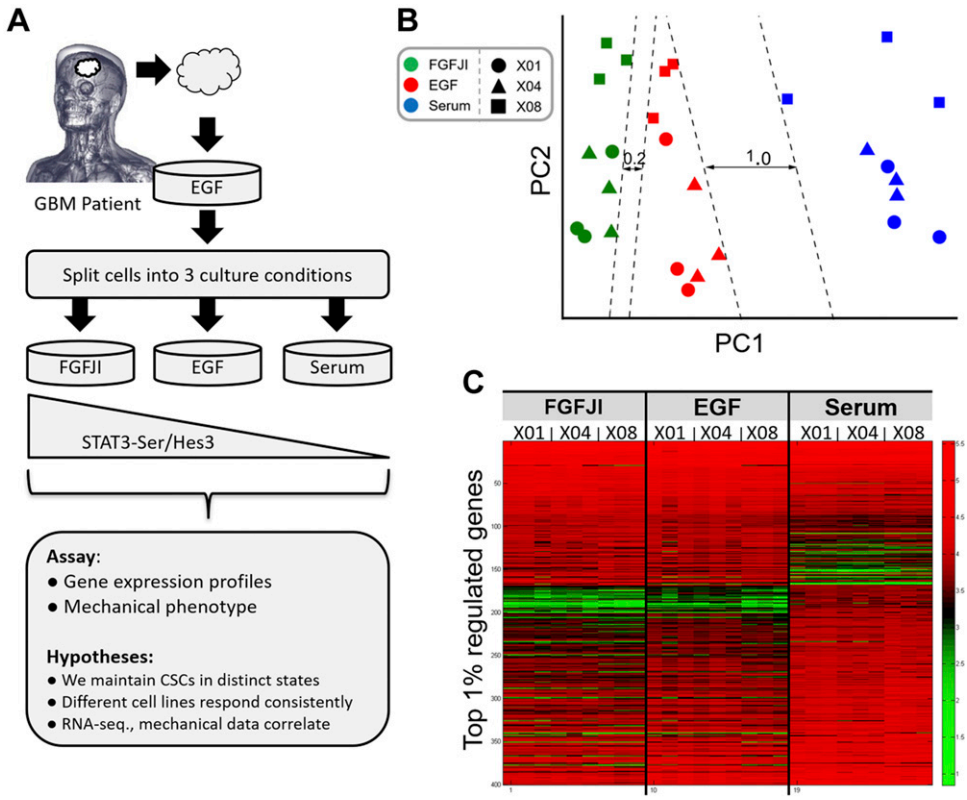

Figure 1. Modeling different cell growth states *in vitro*. *A*) Three different primary brain tumor cell lines (each from a different patient) were established following surgical excision and propagated in serum-free medium containing EGF. Cells were then passaged into new flasks, each containing the same base medium formulation but supplemented with different factors (FGFJI, EGF, or serum). After 5 d, cells were collected for either gene expression profiling or real-time DC. *B*) Plot of PCA shows a patient discriminative pattern of culture condition (PC1) *vs.* patient cell line (PC2). Numbers indicate support-vector machine maximum-margin computation values among the 3 culture condition groups. *C*) Heat map of the top 1% regulated genes.

were selected (201 unique genes). Search Tool for the Retrieval of Interacting Genes/Proteins was used to build the PPI network (200 genes recognized). Experimental evidence with a high confidence score (0.7) was used. The network includes genes whose products are directly regulated by mitogens, including those used in our culture conditions (bFGF, EGF), small G proteins, and cell surface markers implicated in cancer growth. Although we adopted stringent criteria to select the genes and build a mechanomic-related network, we still identified 5 core functional subnetwork modules differentially represented between FGFJI and EGF (**Fig. 2**). Among them, module 3 appears more complete (9 genes in total) and well defined, and it is strongly related to the regulation of cytoskeletal properties, which is important in the modulation of cell-mechanical phenotypes. In particular, we note that this module is composed of 2 different types of nodes that are highlighted in the bar plot beside the PPI. The first type (which comprises 2 genes) is composed of EGFR and microtubule-associated protein 2, share the same pattern, and are more highly expressed in FGFJI than EGF. The second type (which comprises 7 genes) is composed of all the other genes in the module and is expressed at lower levels in FGFJI than in EGF.

These results point to distinct differences between cells cultured in the presence of FGFJI *vs.* EGF.

Mechanomics regulation under different culture conditions

Our gene expression data showed that the culture conditions we used regulate cell mechanics pathways. To address this further, we performed an analysis of the mechanical phenotype using real-time DC (28) to quantify cell size (cross-sectional area) and deformation under hydrodynamic shear stress in a microfluidic channel in each cell line and in each culture medium. Example images demonstrate the specific manner by which all 3 cell lines respond to the 3 different culture conditions (**Fig. 3*A***). The different cell culture conditions were associated with a specific morphologic phenotype, which was similar among the 3 different cell lines. In FGFJI, cells from all 3 patients were smaller in size; in EGF, all 3 were larger; and in serum-containing medium, all 3 were significantly larger still.

When the data is plotted as deformation *vs.* cell area, again, there is an obvious grouping depending on cell culture medium (Fig. 3*B, C* and Supplemental Fig. S1), meaning that cell culture conditions affect the mechanical phenotype of the cells similarly across different cell lines.

The specific manner in which culture conditions affect both gene expression and mechanical phenotype prompted us to quantify this correlation. Because the size of the cell and its deformation in the channel are not independent, we calculated the apparent elastic modulus for each cell (a means of combining size and deformation into 1 value), assuming an isotropic, homogeneous elastic object, according to Mietke *et al.* (29). We plotted the average elastic modulus *vs.* PC1 for each condition (Fig. 3*D*) to determine a possible correlation (linear regression of the normalized PC1 *vs.* elastic modulus variables). The analysis demonstrates significant correlation ($P < 0.001$; linear regression correlation coefficient $R = 0.92$) between the 2 variables, indicating a high correlation between the genomic pattern and the cell mechanics. Indeed, there was again a grouping of all 3 cell lines based on culture condition.

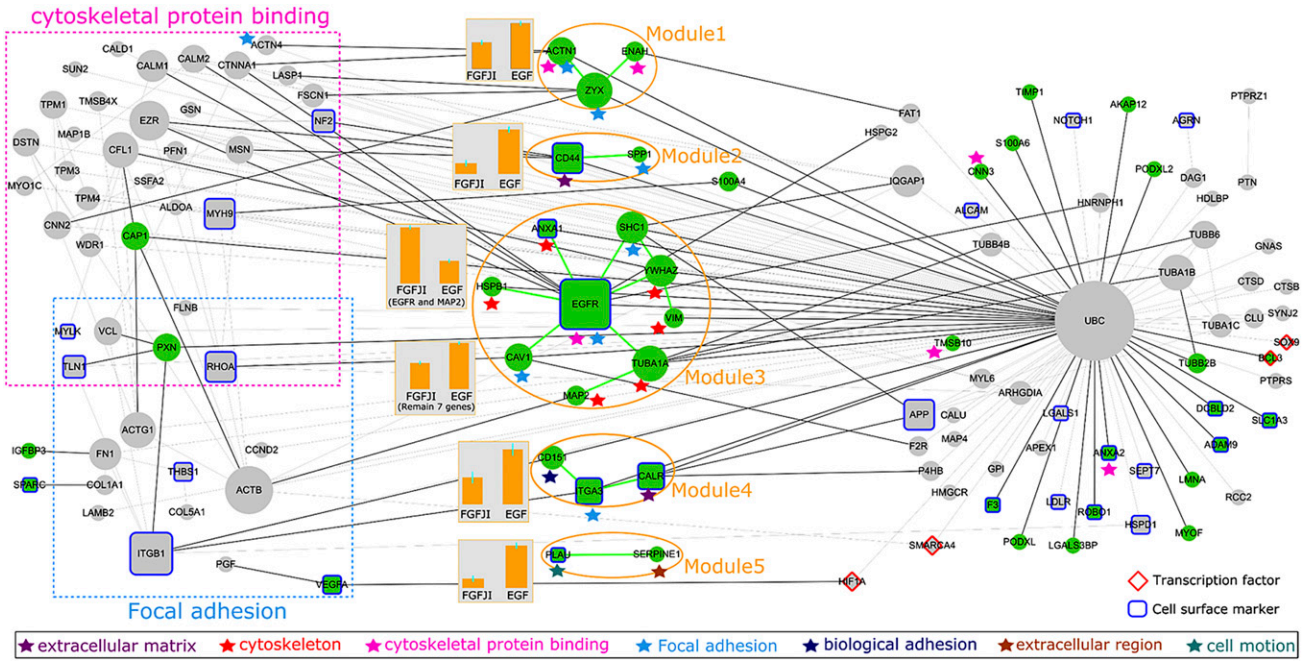

Figure 2. Mechanomics network based on genes regulated by culture conditions. Gene network diagram generated by the top 1% regulated genes between FGFJI *vs.* EGF that belong to mechanics-related functional terms. Green color denotes the differentially expressed functional subnetwork modules of genes and gene links that are significantly different between FGFJI and EGF culture conditions in all 3 cell lines (each from a different patient). Blue borders denote cell surface proteins. Red borders denote transcription factors. Dashed lines depict the most significant functional terms, and the stars indicate the primary functional terms to which each gene belongs.

Gene expression regulation by *HES3* RNA interference

HES3 RNA interference opposes the growth of all 3 primary cell lines used here when cultured in FGFJI (3), pointing to possible core molecular mechanisms that may be targeted in oncology. Here, we set out to identify the genes and signaling pathways affected by *HES3* RNA interference *in vitro* that are common in all 3 cell lines and which may provide therapeutically amenable putative drug targets and biomarkers.

We cultured the X01, X04, and X08 cell lines under the FGFJI conditions (*i.e.*, under conditions that maintain high *HES3* expression). We then performed RNA interference with an siRNA that has been previously validated to oppose *HES3* expression and cell viability (3). Twenty-four hours later, we collected RNA for transcriptomics analysis by RNA sequencing methods.

HES3 RNA interference induced gene-expression changes in all 3 cell lines. We focused on those genes that were significantly regulated at least 2-fold from control (scrambled) siRNA (log2-fold change cutoff, with an adjusted $P < 0.05$). There were 290 differentially regulated genes for X01, 449 for X04, and 56 for X08. Twenty-five genes were common to all 3 cell lines (triple-common) (**Fig. 4*A–C*** and **Table 1**).

We found 3 GO term categories that were regulated in all 3 cell lines by *HES3* siRNA (GO:0005654 ~ nucleoplasm, GO:0005515 ~ protein binding, GO:0005737 ~ cytoplasm). Additional GO terms were found regulated when only the X01 and X04 cell lines were used in the analysis, of which GO:0006260 ~ DNA replication, GO:0051301 ~ cell division, and GO:0006281 ~ DNA repair are noteworthy (Supplemental Fig. S2 and Supplemental Table S3).

An unsupervised comparison of the 2 experiments (gene regulation by cell culture condition and gene regulation by *HES3* RNA interference) allows us to identify the major determinants of gene expression (Fig. 4*D*). The data reveal that culture conditions induce vast differences in gene expression but that *HES3* RNA interference also induces significant changes across the 3 cell lines.

Comparative drug screening in 2 culture conditions

The different gene expression and mechanomics properties that the cells exhibit when placed in different conditions suggested that their response to treatment with small molecules may also differ under different culture conditions. Drug screening the same cell line under different culture conditions may help identify putative drugs that would otherwise be missed.

To address this hypothesis, we used the widely available human brain tumor cell line U-87MG. We chose 2 cell culture conditions: FGFJI and the commonly used serum-supplemented RPMI medium (*i.e.*, the 2 culture conditions with the largest difference in *HES3* expression).

U-87MG cells grow efficiently in both medium formulations. **Figure 5*A*** shows image examples from 1- and 8-d cultures in both mediums. The morphology of the cells

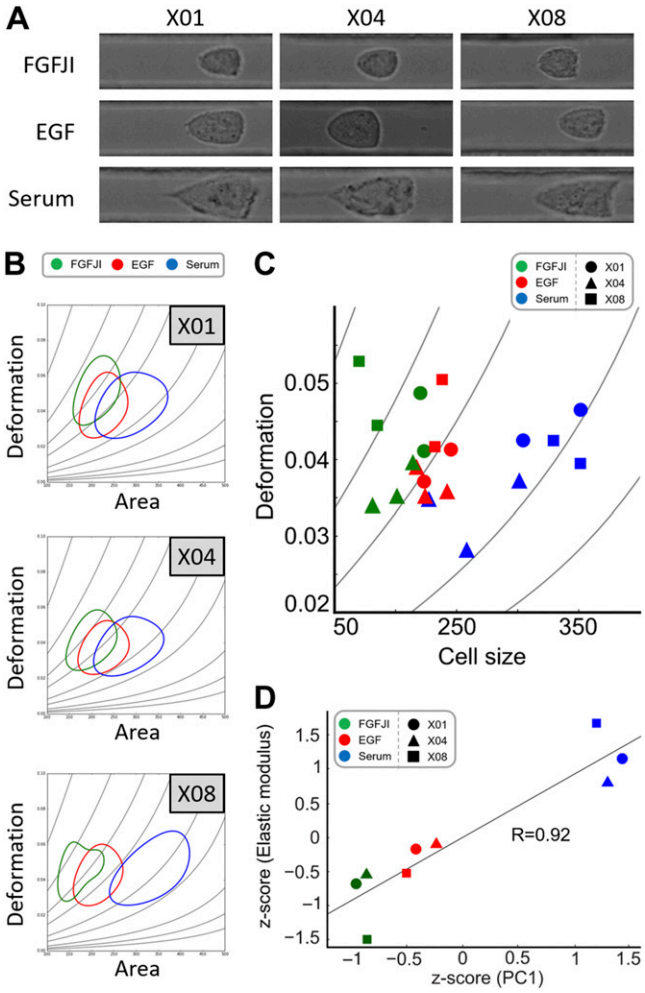

Figure 3. Distinct mechanical phenotypes of cells cultured in different conditions. *A*) Representative images from the different cell lines in the different culture conditions obtained by real-time DC. *B*) Plot of deformation *vs.* cell size for each cell line in each culture condition. The data show the mode values of the distributions of thousands of individual cells analyzed for each condition and patient cell line; isoelasticity lines (gray) show places of equivalent elastic modulus. *C*) Plot of deformation *vs.* cell size for each cell line in each culture condition. The data show the mode values of the distributions of thousands of individual cells analyzed for each condition and patient cell line; isoelasticity lines (gray) show places of equivalent elastic modulus. *D*) Linear regression plot of *z*-score (PC1) and *z*-score (elastic modulus) for each cell line in each culture condition. The PC1 coordinate of each symbol is obtained as the average of the PC1 coordinates of the same respective symbols in Fig. 1*B*. The elastic modulus coordinate of each symbol is calculated as the average of the elastic moduli of the respective symbols in *B*. Both coordinates are *z*-score transformed to adjust for the different physical scales.

differs in the 2 mediums, with FGFJI inducing a smaller and more neural stem cell–like morphology. PCR analysis demonstrated that cells in FGFJI express higher levels of *HES3* than in RPMI (Fig. 5*B*). Cells cultured in FGFJI were also more susceptible to death following *HES3* RNA interference (Fig. 5*C*). One day after transfection, cell number in FGFJI was at 21.0% ± 6.8, relative to control (scrambled)-transfected cells (100% ± 16.8), with a significant value of $P = 3.5 \times 10^{6}$ (Student's *t* test). Cell number in RPMI was at 48.3% ± 25.0, relative to control (scrambled)-transfected cells (100% ± 34.2), with a significant value of $P = 0.0029$ (Student's *t* test).

We screened a library of 1600 FDA-approved compounds at 2 different concentrations (10 and 3 μM) on U-87MG cells cultured in FGFJI (**Fig. 6*A***). The compounds that significantly reduced cell number were then rescreened, in parallel, with the U-87MG cells cultured in both FGFJI and serum conditions. In this way, we identified 37 compounds that only reduced cell number in FGFJI conditions (**Table 2**).

As a final confirmation, we chose 6 compounds for dose curve assays in both FGFJI and serum conditions. Of these, 4 compounds (marked by arrows in the figure) showed a greater effect in FGFJI than in serum (Fig. 6*B*, *C*).

Computational analysis of selected compounds

The 6 compounds selected for dose curve experiments cover 6 different chemical scaffolds, thus providing broad diversity. To get an overview of the compounds, we performed a clustering based on the structural similarity of the 37 compounds (Supplemental Fig. S3). The heat map reveals that the 37 compounds cover structurally very diverse scaffolds and that there are 4 larger groups of very closely related compounds and many singletons (Table 2). For example, the first group, dichlorophenylethylimidazole, comprises 6 compounds, which contain an imidazole group and some chloro groups. These compounds have an antifungal effect and are used in different indications. Chemical structures for these groups are provided (Supplemental Fig. S4).

We analyzed the disease indications of the 37 compounds. In total, they cover a broad spectrum, including anticancer, antipsychotic, antihistamine, anti-inflammatory, laxative, and sleep agents. However, there was a particularly strong focus on anthelmintic, antifungal, and antibiotic actions for 19 of the 37 compounds (Table 2 and Supplemental Fig. S5). With this analysis, we generated a complete drug target–disease network (Supplemental Fig. S6) and a drug–drug target network (Supplemental Fig. S7).

DISCUSSION

In this study, we characterize a distinct signal transduction state of cultured cancer cells derived from patients with aggressive gliomas. We demonstrate that cells from different patients behave similarly in terms of their gene expression regulation when placed in different culture medium, their mechanical phenotype, and their response to *HES3* RNA interference. We utilize these concepts to screen drugs that specifically affect the growth of cells when they are maintained in this distinct state. Our strategy may be incorporated into large-scale screening programs to identify additional putative compounds by screening new drugs or rescreening old drugs and other putative treatments. It may also be integrated into personalized medicine programs aimed at targeting this particular cell state characterized by

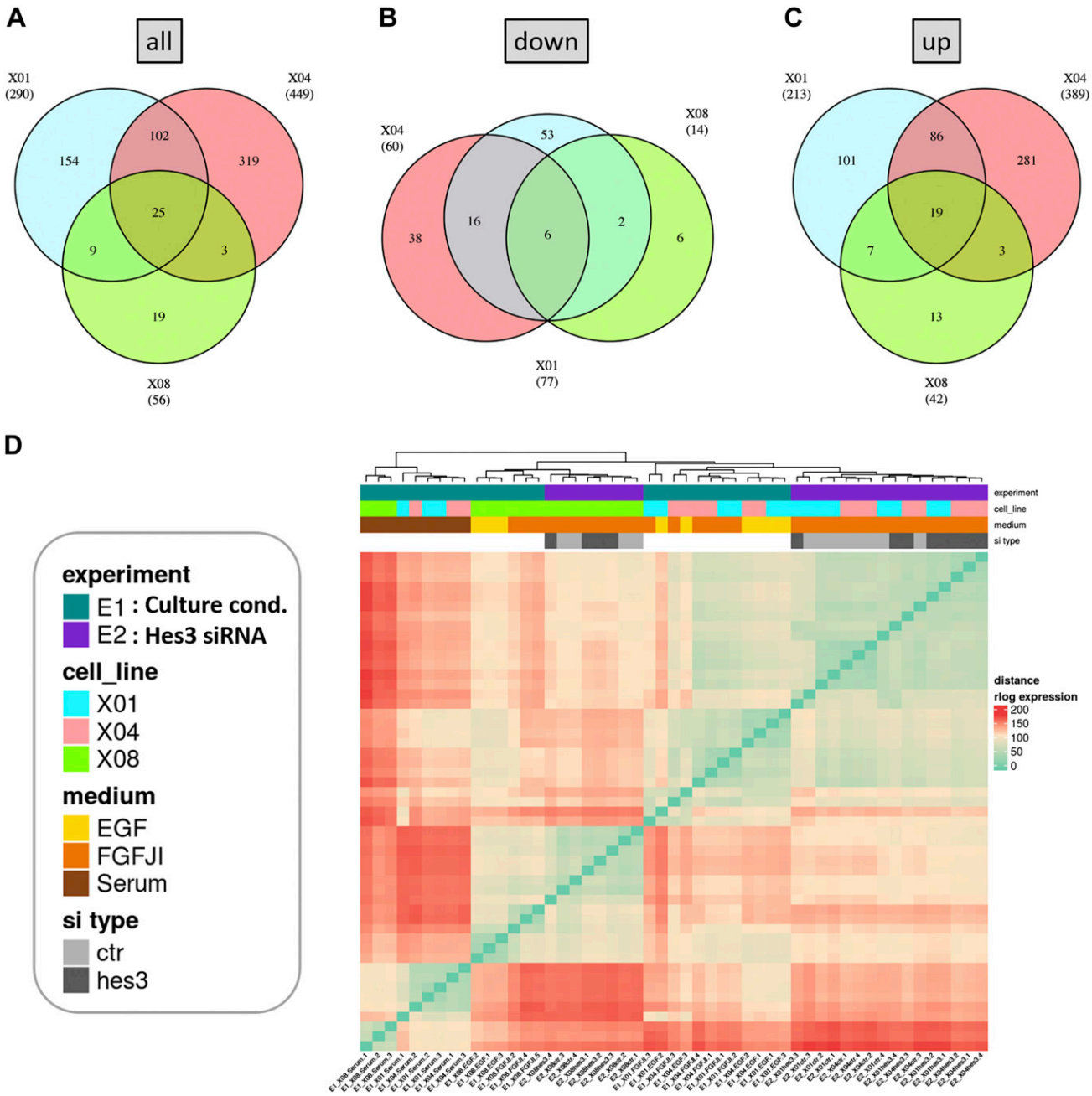

Figure 4. Gene expression regulation following *HES3* RNA interference. *A–C*) Number of genes regulated by *HES3* siRNA in each of the 3 cell lines compared with control (scrambled) siRNA [abs(log2-fold change) >1, and adjusted $P < 0.05$]. Data are split into all genes regulated (*A*), down-regulated genes (*B*), and up-regulated genes (*C*). *D*) Unsupervised clustering heat map of Euclidian sample distances based on all genes' expression.

a distinct gene expression or biomarker profile and response to various treatments.

The *HES3*+ cell state operates in many *in vitro* paradigms

The *HES3*+ cell state has been described in several cell types in culture, including primary and induced pluripotent stem cell (iPS)-derived neural stem cells, mouse insulinoma cells, oligodendrocyte progenitor cell lines, and bovine adrenomedullary chromaffin progenitors (4, 34–38). The pattern of expression of *HES3* supports a role in maintaining the stem cell state. Human embryonic stem cells express *HES3*; when they are induced to differentiate into neurons, they progressively lose *HES3* expression (39). Mouse embryonic feeder cells do not express *HES3*, at least in the serum-containing medium that they are cultured in. When they are reprogrammed into iPS cells, *HES3* expression is induced, peaking at the latest stages of reprogramming; then, as the cells are passed into serum-containing medium to maintain them as stable iPS cell lines, *HES3* expression is lost (39). These results show that the *HES3*+ state can be assumed by different cell types and that these are often plastic cell types, such as various types of stem cell.

TABLE 1. *Triple-common regulated genes in the cell lines X01, X04, and X08 following HES3 RNA interference (log2 fold change, adjusted $P < 0.05$)*

Ensembl_ID	Gene_symbol	Description
Up-regulated by *HES3* siRNA		
ENSG00000167460	*TPM4*	Tropomyosin 4
ENSG00000254332	*GS1-44D20.1*	
ENSG00000089597	*GANAB*	Glucosidase-α; neutral AB
ENSG00000171700	*RGS19*	Regulator of G-protein signaling 19
ENSG00000204611	*ZNF616*	Zinc finger protein 616
ENSG00000213846	*AC098614.2*	
ENSG00000101255	*TRIB3*	Tribbles pseudokinase 3
ENSG00000158373	*HIST1H2BD*	Histone cluster 1, H2bd
ENSG00000128165	*ADM2*	Adrenomedullin 2
ENSG00000139269	*INHBE*	Inhibin, β E
ENSG00000070669	*ASNS*	Asparagine synthetase (glutamine-hydrolyzing)
ENSG00000272405	*RP11-284F21.10*	
ENSG00000100889	*PCK2*	Phosphoenolpyruvate carboxykinase 2 (mitochondrial)
ENSG00000182459	*TEX19*	Testis expressed 19
ENSG00000261371	*PECAM1*	Platelet/endothelial cell adhesion molecule 1
ENSG00000138678	*AGPAT9*	1-acylglycerol-3-phosphate *O*-acyltransferase 9
ENSG00000105550	*FGF21*	Fibroblast growth factor 21
ENSG00000235513	*RP4-756G23.5*	
ENSG00000272068	*RP11-284F21.9*	
Down-regulated by *HES3* siRNA		
ENSG00000181061	*HIGD1A*	HIG1 hypoxia inducible domain family, member 1A
ENSG00000160877	*NACC1*	Nucleus accumbens associated 1, BEN and BTB (POZ) domain containing
ENSG00000171150	*SOCS5*	Suppressor of cytokine signaling 5
ENSG00000258016	*HIGD1AP1*	HIG1 hypoxia inducible domain family, member 1A pseudogene 1
ENSG00000072401	*UBE2D1*	Ubiquitin-conjugating enzyme E2D 1
ENSG00000248785	*HIGD1AP14*	HIG1 hypoxia inducible domain family, member 1A pseudogene 14

Roles of *HES3* in regeneration and cancer

Data from the Human Protein Atlas support a role of *HES3* in maintaining the undifferentiated state. Out of over 60 human cell lines, only 2 show detectable *HES3* RNA expression: the human neuroepithelial stem cell line AF22 and the pluripotent human embryonal carcinoma cell line NTERA-2. One may question if the broad lack of *HES3* expression is due to cell-intrinsic reasons in the cell types assessed or to the culture medium used. Case in point, the Protein Atlas data reports no *HES3* expression in the U-87MG cell line (cultured in serum). These data are in accordance with our finding that although we detect some *HES3* RNA in serum (using PCR), expression levels are low, and we detect significantly more expression when the cells are cultured in FGFJI. This result suggests that assessment of the expression of *HES3* in cell lines must consider the culture systems employed. It will be very useful to determine how many cell types can assume the *HES3*+ state; it might be a common ability that we simply have not yet broadly revealed.

The immediate and obvious question is, what is the relevance of the *HES3*+ state in the tissue and, more specifically, in cancer? There are many lines of evidence that demonstrate roles of *HES3* during development, in the regeneration of tissues in the adult, and in carcinogenesis, which are summarized below.

HES3 and other members of the *Hes/Hey* gene family play important roles in neural development; *HES3* contributes to the maintenance of the isthmic organizer and the development of the mid/hindbrain (2, 40, 41). *HES3*+ neural stem cells can also be found in the adult mammalian brain (4, 42). Oligodendrocyte progenitors also express *HES3* in the adult mammalian brain (38). Beyond the brain, *HES3*+ cells are also found in the pancreas (a significant percentage of β-cells express *HES3*) (34, 43) and the adrenal gland [*HES3* expression has been reported in adrenomedullary chromaffin progenitors of the medulla and the zona glomerulosa of the adrenal cortex, where cortical stem cells are thought to reside (35, 44)].

Studies in which tissues are subjected to injury further support a role of *HES3* in regeneration. Oligodendrocyte damage in the brain by the toxin cuprizone and pancreatic islet damage by the toxin streptozotocin strongly induce *HES3* expression; more importantly, *HES3*-null mice exhibit impaired regeneration in these tissues (34, 38, 43).

Regarding roles of *HES3* specifically in cancer, multiple papers have made the case that *HES3* could become an important new target in cancer therapy. We showed that the 3 primary glioma cell lines used in this paper can be cultured under conditions that maintain *HES3* expression and that, in these conditions, the cells can be killed by *HES3* siRNA (3); moreover, *HES3* is expressed in several human cancers (3). In breast cancer xenotransplantation experiments, human cell lines do not express detectable *HES3* in serum-containing culture conditions but acquire *HES3* expression once grafted into the host animal; *HES3* expression predicts the anticancer efficacy of a γ-secretase inhibitor *in vivo* (45). Experiments with STAT3 phosphorylated mutant plasmids show that STAT3 serine-phosphorylated (an upstream component of the STAT3 serine-phosphorylated/*HES3* signaling pathway) (4) promotes prostate carcinogenesis *in vivo*

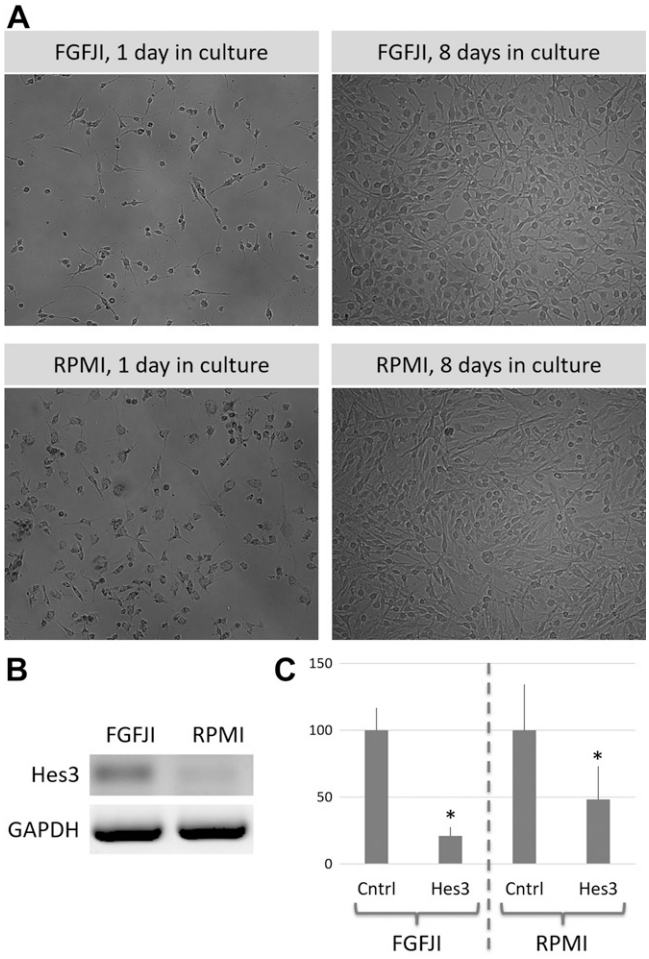

Figure 5. U-87MG cells in different culture conditions. *A*) U-87MG cells grow efficiently in both common medium (RPMI supplemented with serum) and FGFJI medium. Images are from d 1 and 8 in culture and show morphologic differences in the 2 medium compositions (image width: 1.22 mm; the image was acquired with a ×10 objective; the resolution is 0.91 μm/pixel and the image dimensions are 1344×1024 pixels). *B*) PCR analysis shows higher expression of *HES3* in FGFJI than in serum-containing RPMI. Data are from 5 d cultures; Glyceraldehyde 3-phosphate dehydrogenase (GAPDH) is used as the housekeeping gene. *C*) *HES3* RNA interference opposes cell number in both FGFJI and serum-containing RPMI medium but more so in FGFJI. Data are from 1 d post-transfection.

(46). A recent study on the molecular mechanisms behind rhabdomyosarcoma tumorigenesis (a pediatric soft-tissue sarcoma often caused by PAX3-FOXO1 fusion) showed, using a new genetic fish model, that human *HES3* inhibits *in vivo* myogenesis and supports inappropriate persistence of PAX3-FOXO1+ cells and that *HES3* overexpression increases protumorigenic features in cell culture systems (47). The same authors also demonstrated, through analysis of data from rhabdomyosarcoma patient cohorts, that *HES3* expression correlates with poor patient survival in the PAX3-FOXO1+ tumors.

Taken together, these studies show that *HES3* and its regulators or mediators are important components of tissue repair and become deregulated in cancer. Cell systems that are currently used for research and drug discovery can assume both the *HES3*− and the *HES3*+ states. Because *HES3* is associated with the maintenance of the stem cell state, treatments against the *HES3*+ state might be particularly important because they might target the most plastic cancer cell types that are difficult to target with current methods (48).

In this paper, we took the approach of targeting a cancer cell state as opposed to a specific molecule or signal transduction pathway that is important for the growth of cancer cells. We envision future therapeutic strategies that will combine specific targeting of the *HES3* signaling pathway (*e.g.*, by *HES3* siRNA) (3) with drugs, such as those identified here, that are particularly effective at killing cells that operate the *HES3* signaling pathway.

It is not clear, at this stage, whether the drug screening results we identified interfere, directly or indirectly, with the *HES3* signaling pathway. To address this, it will help to identify additional drugs that specifically target the *HES3*+ state by performing larger screens and to incorporate the *HES3* signaling pathway in existing signal transduction databases, such as KEGG.

It will also help to determine what genes are regulated by the drug hits in the different culture conditions. It is possible that the data sets from the different culture conditions will be quite different from each other but that common genes (or GO terms) will be regulated by various drugs in the FGFJI conditions, providing clues to the mode of action of these drugs regarding their potential new purpose.

It is possible that multiple cellular mechanisms might mediate anticancer effects *via* either *HES3* siRNA or the small molecules we identified. Hes3 RNA interference leads to the death of multiple cell types (3, 34), and recently, Hes3 was implicated in the regulation of cell proliferation and cell invasion in lung cancer cell lines (49). Our observation that cell mechanics–related GO terms were strongly featured in the PC analysis is consistent with the latter point. It is possible, therefore, that targeting Hes3 might be an effective strategy that is not limited to the fast proliferating cancer cell population. It will be very important, therefore, to assess the efficacy of these treatments not simply by their ability to kill a large number of cancer cells but by assessing whether they can kill therapy-evading cells. *HES3* might be a core component of the intersection among development, regeneration, and cancer in various tissues.

Screening in the *HES3*+ state

Although it will be impossible to find any cell culture system that is not plagued by artifact, understanding, at the molecular level, the various growth options that cancer cells have at their disposal and developing cell culture systems to model, study, and use them in drug screening can lead to the discovery of new drug uses in oncology. Here, we present proof-of-concept data and a strategy that can be scaled up to screen and rescreen vast libraries of compounds. Our method will significantly increase the value of large-scale screens (50) aimed at prioritizing putative cancer therapeutic targets because the results are likely going to be very different if the screen is performed

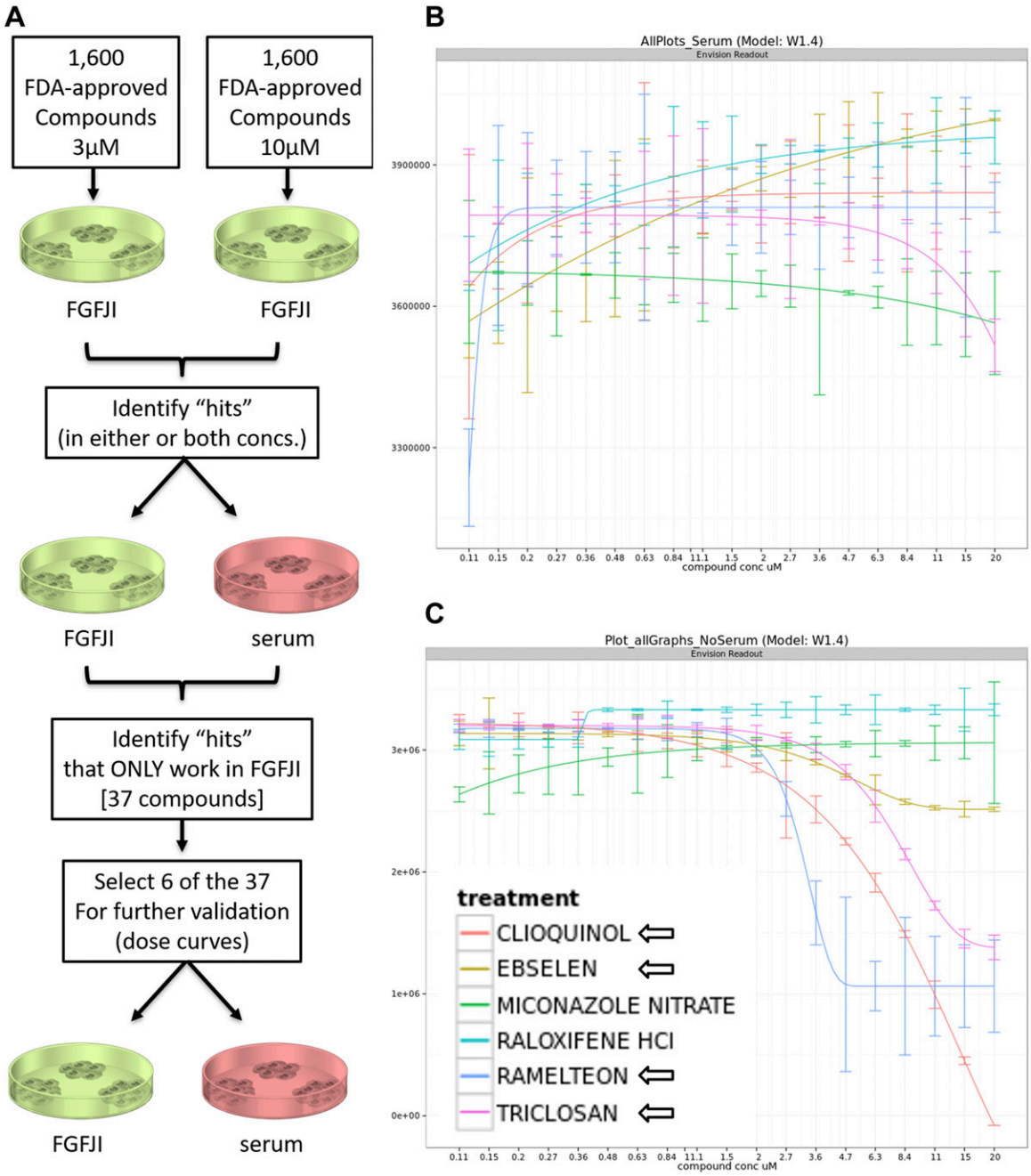

Figure 6. Drug screening in different culture conditions. *A*) The drug screening strategy. *B*) Dose curves of 6 selected compounds in the serum-containing cell culture condition. *C*) Dose curves of the same 6 selected compounds in the FGFJI cell culture condition. Arrows point to the 4 of the 6 compounds used in the dose curve experiment that demonstrated efficacy in FGFJI but not in serum.

in cell culture conditions that maintain the expression and operation of Hes3 than if it is performed under the more common, serum-containing conditions that suppress Hes3 expression.

We selected culture conditions that allow us to lock cells in 3 distinct states regarding *HES3* expression (3). Our aim is not to study the molecular mechanisms downstream of particular cytokines that are included in the culture medium but rather to study the same cells under different states. This strategy revealed that many of the genes regulated by culture condition relate to the mechanical properties of the cells, prompting us to measure their mechanical phenotype. Cancer cells can be characterized by their mechanical signature, being more deformable than healthy counterparts, as has been established for many cell lines and primary cells from many different tumor types, including primary oral squamous cell carcinomas (51, 52). A notable exception seems to be leukemia, in which the cancer cells are stiffer (53). Again, all 3 cell lines behaved similarly to each other, and we identified a strong correlation between the *HES3*+ state and small or deformable cells. Likewise, the primary cell lines behaved similarly in terms of their gene expression profile when treated with a *HES3* siRNA product.

TABLE 2. *List of 37 compounds (from a library of 1600 FDA-approved compounds) that reduce cell number in FGFJI but not in serum culture conditions with disease indication, number of targets, and protein structures*

Compound #	Name	Group	CID	Disease/effect	Target	Structure
1	Butoconazole	1	47472	Antifungal	1	0
2	Sulconazole	1	5318	Antifungal	12	0
3	Tioconazole	1	5482	Antifungal	1	0
4	Oxiconazole	1	5353853	Antifungal	2	0
5	Econazole	1	3198	Antifungal	20	4
6[a]	Miconazole	1	4189	Antifungal	27	0
7	Lasalocid	S	5360807	Antibiotic	0	1
8	Quinestrol	S	9046	Anticancer	0	0
9	Oxyclozanide	2	16779	Anthelmintic	0	0
10	Clofoctol	2	2799	Antibiotic	0	0
11	Dichlorophen	2	3037	Anticestodal	2	0
12	Bithionol (bithionate Na)	2	2406	Anthelmintic	12	2
13[a]	Triclosan	2	5564	Antibiotic	16	31
14	Ritonavir	S	392622	Antiretroviral	23	15
15	Vinblastine	S	13342	Anticancer	13	4
16	Bisacodyl	S	2391	Laxative	2	0
17	Diltiazem	S	39186	Blood pressure treatment	15	0
18[a]	Raloxifene hydrochloride	S	5035	osteoporosis	21	5
19	Benzethonium	S	2335	Antimicrobial	0	0
20[a]	Ramelteon	S	208902	Sleep agent	2	0
21	Levocetirizine	S	1549000	Antihistamine	1	1
22	Suloctidil	S	5354	Blood pressure treatment	0	0
23[a]	Ebselen	S	3194	Anti-inflammatory	26	0
24	Pimozide	S	16362	Antipsychotic	47	0
25	Chlorhexidine	S	53589	Antimicrobial	0	0
26	Xylazine	S	5707	Anesthesia	5	0
27	Chloroxine	3	2722	Antibiotic	9	0
28[a]	Clioquinol	3	2788	Antifungal	13	1
29	Broxaldine	3	77262	Antiprotozoal	0	0
30	Broxyquinoline	3	2453	Antiprotozoal	1	0
31	Hexetidine	S	3607	Antibiotic	0	0
32	Norethynodrel	S	6231	Oral contraceptive	1	0
33	Sodium aescinate	4	3084345	Lung injury treatment	0	0
34	Abamectin	4	71312393	Anthelmintic	0	0
35	Doramectin	4	11954226	Anthelmintic	0	0
36	Milbemycin	4	6436009	Anthelmintic	0	0
37	Selamectin	4	6445091	Anthelmintic	0	0

CID, compound identification number; S, singleton (*i.e.*, compounds that do not belong to one of the defined groups). [a]Compounds further tested in dose experiments.

Despite these similarities among different cell lines, nuanced differences may help with an integrated gene or mechanic patient-specific characterization of their tumor cells. For example, the X08 cell line showed differences in gene expression patterns compared with X01 and X04. In the PC analysis, data from the X08 cell line are separated from the data from the X01 and X04 cell lines, which tend to cluster together. X08 cells were derived from a patient with gliosarcoma, whereas X01 and X04 cells were from 2 patients with glioblastoma. Future studies with a larger number of patient-derived cell lines may address whether gene expression analyses like the one performed here might help with the categorization of glioma subtypes. Also, in the serum conditions (that likely represent the differentiated state of the cells), the X08 line exhibits greater variance in the gene expression data. It will be interesting to address whether this observation represents a greater differentiation potential of these cells in accordance with the notion that aggressive tumors contain more primordial cancer stem cell types that evade therapy (gliosarcomas are particularly aggressive) (54). The methods employed in this work appear very sturdy; differences between X08 and the other 2 primary cell lines were picked in both the gene expression data and the mechanomics analyses.

Following characterization of the different signaling states in the 3 primary human brain tumor cell lines, we switched to the broadly available human brain tumor cell line U-87MG to identify drugs that specifically kill cells in the *HES3*+ state. This will help other laboratories reproduce the data we present. Because the *HES3*+ state is largely overlooked, we hypothesized that this strategy could identify potentially very valuable drugs for repurposing. Starting with a 1600 FDA-approved compound library, we identified 37 compounds that are effective at reducing cell number only or significantly more in FGFJI as opposed to in serum. We selected 6 of these compounds for further confirmation, producing dose curve data in the 2 cell culture conditions. Of the 6 compounds, 4 (clioquinol, ebselen, ramelteon, and triclosan) were successfully

validated, providing stringent proof of principle for the efficacy of this screening strategy.

The results from the screening assay represent diverse chemical groups

Our screening assay strategy was designed to interrogate a cell state as opposed to a specific molecular target. Perhaps not surprisingly, then, the hits represented a wide range of chemical scaffolds. How does the diversity in compound scaffolds relate to the targets of the drugs? In one extreme scenario, each drug would hit its own targets; at the other extreme, all drugs would bind to the same targets. To address this question, we retrieved drug-target data from BindingDB. Many of the drug results are promiscuous. For example, Table 2 shows that the antipsychotic pimozide, which is used in schizophrenia and psychosis, has 47 targets listed in BindingDB. This holds true for many of the other compounds, too; 18 out of the 37 compounds have more than 1 target. Supplemental Figure S7 shows the network between compounds and targets. The figure reveals that groups of related compounds generally hit similar targets. Overall, there are 178 targets, which are hit by at least 2 of the 37 compounds. This means that there is neither 1 common mode of action for the identified compounds, nor do they all exhibit very individual, isolated effects. Instead, there are some commonalities and many differences between the compounds. Among the common targets hit by many drugs, are, for example, the multidrug-resistant (MDR) proteins MDR1, MDR1A, and MDR1B (Uniprot ID: P08183, P21447, P06795). They bind miconazole in the imidazole group, the antipsychotic pimozide, the HIV drug ritonavir, and the anticancer drug vinblastine. These MDR proteins are ATP-dependent efflux pumps with a broad substrate specificity for the transport of endogenous and xenobiotic anionic substances localized in cellular plasma membranes. Similarly, the protein cytochrome P450 3A4 (Uniprot: P08684) binds 7 compounds: the antifungals miconazole and econazole and the singletons raloxifene, pimozide, diltiazem, ritonavir, and vinblastine. Cytochrome P450 is known to perform a variety of oxidation reactions of structurally unrelated compounds, which explains the links to different compounds in the data set. The protein indoleamine 2,3-dioxygenase 1 (Uniprot: P14902, E5RGR8, and P28776) is linked to 5 compounds belonging to group 1 (econazole, miconazole, sulconazole, and oxiconazole) and group 2 (dichlorophen). The protein is an enzyme in the tryptophan catabolism pathway related to depletion of tryptophan, which can cause halted growth of microbes as well as T cells. Emerging evidence suggests that indoleamine 2,3-dioxygenase 1 becomes activated during tumor development, helping malignant cells escape eradication by the immune system. The protein nuclear receptor subfamily 1 group I member 2 (Uniprot: O75469) is linked to 4 compounds belonging to group 2 (bithionol), group 3 (chloroxine), and singletons (raloxifene and ritonavir). It is a nuclear receptor that binds to and is activated by a variety of endogenous and xenobiotic compounds.

Ideally, appropriate drug hits will be tested in clinical trials to prove their therapeutic potential. Ramelteon is a melatonin receptor agonist used as a sleep agent. It was recently shown to suppress the proliferation and invasiveness of cultured endometrial cancer cells (55). Melatonin itself has been suggested as a possible cancer prevention and treatment drug based on epidemiologic and basic studies (56), supporting the potential of our screening strategy. Overall, our work provides a screening platform for the identification of putative anticancer agents, and the basic science on which it is based may help explain the molecular mechanism of such compounds.

A final thought about *HES3* as a target in oncology is that current evidence suggests that the off-target effects may be tolerable. *HES3* is important in tissue regeneration following injury. However, under normal conditions, very few cells express *HES3* postnatally. Accordingly, the *HES3*-null mouse line does not exhibit any significant phenotypes under normal conditions (41). Therefore, it is possible that direct inhibition of *HES3* and/or indirect inhibition by drugs that target *HES3*+ cells may be tolerated by the patient.

Our work uncovers and characterizes a signal transduction state that cancer cells can assume and that renders them sensitive to a different set of treatments than their more established and commonly studied state. These findings may help identify ways to block escape strategies that cancer cells employ to evade current therapies. FJ

ACKNOWLEDGMENTS

The authors are grateful to the Microstructure Facility of Biotechnology Center (BIOTEC)/Center for Regenerative Therapies Dresden (CRTD), Technische Universität Dresden, funded by the Europäischen Fonds für regionale Entwicklung (EFRE) for the production of real-time deformability cytometry microfluidic chips. The Technische Universitaet Dresden has intellectual property (patented and patent-pending) on aspects described in this manuscript for use in oncology (Inventors: A.A.-T. and S.W.P.). J.G. was supported by the Deutsche Forschungsgemeinschaft (Grant KFO249, GU 612/2-2), the Alexander-von-Humboldt Foundation (Humboldt Professorship), and the Sächsisches Ministerium für Wissenschaft und Kunst (Grant TG70). O.O. was supported by the Sächsisches Ministerium für Wissenschaft und Kunst (Grant TG70). C.V.C. was supported by the independent group leader starting grant of the Technische Universität Dresden. A.A.T. was supported by the Deutsche Forschungsgemeinschaft (Grant SFB 655, "Cells into Tissues," Project A24). A.A.T. and S.R.B. were supported by the Deutsche Forschungsgemeinschaft (Grant CRC/Transregio 205/1 and Grant IRTG 2251). A.A.T. and S.R.B. were supported by the TransCampus initiative between Technische Universität Dresden and King's College London and the Transcelerator. O.O. is cofounder at Zellmechanik Dresden (*http://www.zellmechanik.com*). A.A.-T. and S.R.B. are cofounders of Innate Repair (*www.innaterepair.com*). The authors declare no other conflicts of interest.

AUTHOR CONTRIBUTIONS

S. W. Poser, O. Otto, C. V. Cannistraci, J. Guck, and A. Androutsellis-Theotokis designed and performed research, analyzed data, and wrote the manuscript; D. M. Park and A. Mcintyre designed research and wrote the manuscript; C. Arps-Forker, C. Andree, S. Stodolak, and P. Nikolakopoulou performed research; Y. Ge, M. Herbig,

M. F. Adasme, M. Lesche, A. Dahl, and M. Bickle performed research, analyzed data, and helped write the manuscript; and K. Gruetzmann, P. Lennig, S. R. Bornstein, E. Schroeck, B. Klink, R. R. Leker, G. O. Chrousos, and M. Schroeder analyzed data and helped write the manuscript.

REFERENCES

1. Kodack, D. P., Askoxylakis, V., Ferraro, G. B., Sheng, Q., Badeaux, M., Goel, S., Qi, X., Shankaraiah, R., Cao, Z. A., Ramjiawan, R. R., Bezwada, D., Patel, B., Song, Y., Costa, C., Naxerova, K., Wong, C. S. F., Kloepper, J., Das, R., Tam, A., Tanboon, J., Duda, D. G., Miller, C. R., Siegel, M. B., Anders, C. K., Sanders, M., Estrada, M. V., Schlegel, R., Arteaga, C. L., Brachtel, E., Huang, A., Fukumura, D., Engelman, J. A., and Jain, R. K. (2017) The brain microenvironment mediates resistance in luminal breast cancer to PI3K inhibition through HER3 activation. *Sci. Transl. Med.* **9**, eaal4682; erratum: 11, eaal4682
2. Imayoshi, I., and Kageyama, R. (2014) bHLH factors in self-renewal, multipotency, and fate choice of neural progenitor cells. *Neuron* **82**, 9–23
3. Park, D. M., Jung, J., Masjkur, J., Makrogkikas, S., Ebermann, D., Saha, S., Rogliano, R., Paolillo, N., Pacioni, S., McKay, R. D., Poser, S., and Androutsellis-Theotokis, A. (2013) Hes3 regulates cell number in cultures from glioblastoma multiforme with stem cell characteristics. *Sci. Rep.* **3**, 1095
4. Androutsellis-Theotokis, A., Leker, R. R., Soldner, F., Hoeppner, D. J., Ravin, R., Poser, S. W., Rueger, M. A., Bae, S. K., Kittappa, R., and McKay, R. D. (2006) Notch signalling regulates stem cell numbers in vitro and in vivo. *Nature* **442**, 823–826
5. Buchert, M., Burns, C. J., and Ernst, M. (2016) Targeting JAK kinase in solid tumors: emerging opportunities and challenges. *Oncogene* **35**, 939–951
6. Mukthavaram, R., Ouyang, X., Saklecha, R., Jiang, P., Nomura, N., Pingle, S. C., Guo, F., Makale, M., and Kesari, S. (2015) Effect of the JAK2/STAT3 inhibitor SAR317461 on human glioblastoma tumorspheres. *J. Transl. Med.* **13**, 269
7. Androutsellis-Theotokis, A., Rueger, M. A., Park, D. M., Boyd, J. D., Padmanabhan, R., Campanati, L., Stewart, C. V., LeFranc, Y., Plenz, D., Walbridge, S., Lonser, R. R., and McKay, R. D. (2010) Angiogenic factors stimulate growth of adult neural stem cells. *PLoS One* **5**, e9414
8. Brocard, E., Oizel, K., Lalier, L., Pecqueur, C., Paris, F., Vallette, F. M., and Oliver, L. (2015) Radiation-induced PGE2 sustains human glioma cells growth and survival through EGF signaling. *Oncotarget* **6**, 6840–6849
9. Guck, J., Schinkinger, S., Lincoln, B., Wottawah, F., Ebert, S., Romeyke, M., Lenz, D., Erickson, H. M., Ananthakrishnan, R., Mitchell, D., Käs, J., Ulvick, S., and Bilby, C. (2005) Optical deformability as an inherent cell marker for testing malignant transformation and metastatic competence. *Biophys. J.* **88**, 3689–3698
10. Kumar, S., and Weaver, V. M. (2009) Mechanics, malignancy, and metastasis: the force journey of a tumor cell. *Cancer Metastasis Rev.* **28**, 113–127
11. Zhang, W., Kai, K., Choi, D. S., Iwamoto, T., Nguyen, Y. H., Wong, H., Landis, M. D., Ueno, N. T., Chang, J., and Qin, L. (2012) Microfluidics separation reveals the stem-cell-like deformability of tumor-initiating cells. *Proc. Natl. Acad. Sci. USA* **109**, 18707–18712
12. Byun, S., Son, S., Amodei, D., Cermak, N., Shaw, J., Kang, J. H., Hecht, V. C., Winslow, M. M., Jacks, T., Mallick, P., and Manalis, S. R. (2013) Characterizing deformability and surface friction of cancer cells. *Proc. Natl. Acad. Sci. USA* **110**, 7580–7585
13. Soeda, A., Park, M., Lee, D., Mintz, A., Androutsellis-Theotokis, A., McKay, R. D., Engh, J., Iwama, T., Kunisada, T., Kassam, A. B., Pollack, I. F., and Park, D. M. (2009) Hypoxia promotes expansion of the CD133-positive glioma stem cells through activation of HIF-1alpha. *Oncogene* **28**, 3949–3959
14. Soeda, A., Inagaki, A., Oka, N., Ikegame, Y., Aoki, H., Yoshimura, S., Nakashima, S., Kunisada, T., and Iwama, T. (2008) Epidermal growth factor plays a crucial role in mitogenic regulation of human brain tumor stem cells. *J. Biol. Chem.* **283**, 10958–10966
15. Poser, S. W., and Androutsellis-Theotokis, A. (2013) Growing neural stem cells from conventional and nonconventional regions of the adult rodent brain. *J. Vis. Exp.* **81**, e50880
16. Wu, T. D., and Nacu, S. (2010) Fast and SNP-tolerant detection of complex variants and splicing in short reads. *Bioinformatics* **26**, 873–881
17. Liao, Y., Smyth, G. K., and Shi, W. (2014) featureCounts: an efficient general purpose program for assigning sequence reads to genomic features. *Bioinformatics* **30**, 923–930
18. Love, M. I., Huber, W., and Anders, S. (2014) Moderated estimation of fold change and dispersion for RNA-seq data with DESeq2. *Genome Biol.* **15**, 550
19. Cannistraci, C. V., Ravasi, T., Montevecchi, F. M., Ideker, T., and Alessio, M. (2010) Nonlinear dimension reduction and clustering by Minimum Curvilinearity unfold neuropathic pain and tissue embryological classes. *Bioinformatics* **26**, i531–i539
20. Ringnér, M. (2008) What is principal component analysis? *Nat. Biotechnol.* **26**, 303–304
21. Cannistraci, C. V., Alanis-Lobato, G., and Ravasi, T. (2013) Minimum curvilinearity to enhance topological prediction of protein interactions by network embedding. *Bioinformatics* **29**, i199–i209
22. Huang da, W., Sherman, B. T., and Lempicki, R. A. (2009) Systematic and integrative analysis of large gene lists using DAVID bioinformatics resources. *Nat. Protoc.* **4**, 44–57
23. Huang da, W., Sherman, B. T., and Lempicki, R. A. (2009) Bioinformatics enrichment tools: paths toward the comprehensive functional analysis of large gene lists. *Nucleic Acids Res.* **37**, 1–13
24. Szklarczyk, D., Franceschini, A., Wyder, S., Forslund, K., Heller, D., Huerta-Cepas, J., Simonovic, M., Roth, A., Santos, A., Tsafou, K. P., Kuhn, M., Bork, P., Jensen, L. J., and von Mering, C. (2015) STRING v10: protein-protein interaction networks, integrated over the tree of life. *Nucleic Acids Res.* **43**, D447–D452
25. Shannon, P., Markiel, A., Ozier, O., Baliga, N. S., Wang, J. T., Ramage, D., Amin, N., Schwikowski, B., and Ideker, T. (2003) Cytoscape: a software environment for integrated models of biomolecular interaction networks. *Genome Res.* **13**, 2498–2504
26. Luo, J., Kaplitt, M. G., Fitzsimons, H. L., Zuzga, D. S., Liu, Y., Oshinsky, M. L., and During, M. J. (2002) Subthalamic GAD gene therapy in a Parkinson's disease rat model. *Science* **298**, 425–429
27. Gu, Z., Eils, R., and Schlesner, M. (2016) Complex heatmaps reveal patterns and correlations in multidimensional genomic data. *Bioinformatics* **32**, 2847–2849
28. Otto, O., Rosendahl, P., Mietke, A., Golfier, S., Herold, C., Klaue, D., Girardo, S., Pagliara, S., Ekpenyong, A., Jacobi, A., Wobus, M., Topfner, N., Keyser, U. F., Mansfeld, J., Fischer-Friedrich, E., and Guck, J. (2015) Real-time deformability cytometry: on-the-fly cell mechanical phenotyping. *Nature Methods* **12**, 199–202, 4 p following 202
29. Mietke, A., Otto, O., Girardo, S., Rosendahl, P., Taubenberger, A., Golfier, S., Ulbricht, E., Aland, S., Guck, J., and Fischer-Friedrich, E. (2015) Extracting cell stiffness from real-time deformability cytometry: theory and experiment. *Biophys. J.* **109**, 2023–2036
30. Bates, D., Maechler, M., Bolker, B., and Walker, S. (2014) lme4: linear mixed-effects models using Eigen and S4. *R package version* 1
31. Bates, D., Mächler, M., Bolker, B., and Walker, S. (2015) Fitting linear mixed-effects models using lme4. *Journal of Statistical Software* **67**, 1–48
32. Wang, Z., Gerstein, M., and Snyder, M. (2009) RNA-Seq: a revolutionary tool for transcriptomics. *Nat. Rev. Genet.* **10**, 57–63
33. Cortes, C., and Vapnik, V. (1995) Support-vector networks. In *Machine Learning* (Saitta, L., ed.), Vol. 20, pp. 273–297, Kluwer Academic Publishers, Boston
34. Masjkur, J., Arps-Forker, C., Poser, S. W., Nikolakopoulou, P., Toutouna, L., Chenna, R., Chavakis, T., Chatzigeorgiou, A., Chen, L. S., Dubrovska, A., Choudhary, P., Uphues, I., Mark, M., Bornstein, S. R., and Androutsellis-Theotokis, A. (2014) Hes3 is expressed in the adult pancreatic islet and regulates gene expression, cell growth, and insulin release. *J. Biol. Chem.* **289**, 35503–35516
35. Masjkur, J., Levenfus, I., Lange, S., Arps-Forker, C., Poser, S., Qin, N., Vukicevic, V., Chavakis, T., Eisenhofer, G., Bornstein, S. R., Ehrhart-Bornstein, M., and Androutsellis-Theotokis, A. (2014) A defined, controlled culture system for primary bovine chromaffin progenitors reveals novel biomarkers and modulators. *Stem Cells Transl. Med.* **3**, 801–808
36. Salewski, R. P., Buttigieg, J., Mitchell, R. A., van der Kooy, D., Nagy, A., and Fehlings, M. G. (2013) The generation of definitive neural stem cells from PiggyBac transposon-induced pluripotent stem cells can be enhanced by induction of the NOTCH signaling pathway. *Stem Cells Dev.* **22**, 383–396
37. Ohta, S., Misawa, A., Fukaya, R., Inoue, S., Kanemura, Y., Okano, H., Kawakami, Y., and Toda, M. (2012) Macrophage migration inhibitory

factor (MIF) promotes cell survival and proliferation of neural stem/progenitor cells. *J. Cell Sci.* **125**, 3210–3220
38. Toutouna, L., Nikolakopoulou, P., Poser, S. W., Masjkur, J., Arps-Forker, C., Troullinaki, M., Grossklaus, S., Bosak, V., Friedrich, U., Ziemssen, T., Bornstein, S. R., Chavakis, T., and Androutsellis-Theotokis, A. (2016) Hes3 expression in the adult mouse brain is regulated during demyelination and remyelination. *Brain Res.* **1642**, 124–130
39. Poser, S. W., Chenoweth, J. G., Colantuoni, C., Masjkur, J., Chrousos, G., Bornstein, S. R., McKay, R. D., and Androutsellis-Theotokis, A. (2015) Concise review: reprogramming, behind the scenes: noncanonical neural stem cell signaling pathways reveal new, unseen regulators of tissue plasticity with therapeutic implications. *Stem Cells Transl. Med.* **4**, 1251–1257
40. Lobe, C. G. (1997) Expression of the helix-loop-helix factor, Hes3, during embryo development suggests a role in early midbrain-hindbrain patterning. *Mech. Dev.* **62**, 227–237
41. Hirata, H., Tomita, K., Bessho, Y., and Kageyama, R. (2001) Hes1 and Hes3 regulate maintenance of the isthmic organizer and development of the mid/hindbrain. *EMBO J.* **20**, 4454–4466
42. Androutsellis-Theotokis, A., Rueger, M. A., Park, D. M., Mkhikian, H., Korb, E., Poser, S. W., Walbridge, S., Munasinghe, J., Koretsky, A. P., Lonser, R. R., and McKay, R. D. (2009) Targeting neural precursors in the adult brain rescues injured dopamine neurons. *Proc. Natl. Acad. Sci. USA* **106**, 13570–13575
43. Masjkur, J., Poser, S. W., Nikolakopoulou, P., Chrousos, G., McKay, R. D., Bornstein, S. R., Jones, P. M., and Androutsellis-Theotokis, A. (2016) Endocrine pancreas development and regeneration: noncanonical ideas from neural stem cell biology. *Diabetes* **65**, 314–330
44. Nikolakopoulou, P., Poser, S. W., Masjkur, J., Fernandez Rubin de Celis, M., Toutouna, L., Andoniadou, C. L., McKay, R. D., Chrousos, G., Ehrhart-Bornstein, M., Bornstein, S. R., and Androutsellis-Theotokis, A. (2016) STAT3-Ser/Hes3 signaling: a new molecular component of the neuroendocrine system? *Horm. Metab. Res.* **48**, 77–82
45. Zhang, C. C., Pavlicek, A., Zhang, Q., Lira, M. E., Painter, C. L., Yan, Z., Zheng, X., Lee, N. V., Ozeck, M., Qiu, M., Zong, Q., Lappin, P. B., Wong, A., Rejto, P. A., Smeal, T., and Christensen, J. G. (2012) Biomarker and pharmacologic evaluation of the γ-secretase inhibitor PF-03084014 in breast cancer models. *Clin. Cancer Res.* **18**, 5008–5019
46. Qin, H. R., Kim, H. J., Kim, J. Y., Hurt, E. M., Klarmann, G. J., Kawasaki, B. T., Duhagon Serrat, M. A., and Farrar, W. L. (2008) Activation of signal transducer and activator of transcription 3 through a phosphomimetic serine 727 promotes prostate tumorigenesis independent of tyrosine 705 phosphorylation. *Cancer Res.* **68**, 7736–7741
47. Kendall, G. C., Watson, S., Xu, L., LaVigne, C. A., Murchison, W., Rakheja, D., Skapek, S. X., Tirode, F., Delattre, O., and Amatruda, J. F. (2018) *PAX3-FOXO1* transgenic zebrafish models identify *HES3* as a mediator of rhabdomyosarcoma tumorigenesis. *eLife* **7**, e33800
48. Meacham, C. E., and Morrison, S. J. (2013) Tumour heterogeneity and cancer cell plasticity. *Nature* **501**, 328–337
49. Fang, C., Jiang, B., Shi, X., and Fan, C. (2019) Hes3 enhances the malignant phenotype of lung cancer through upregulating Cyclin D1, Cyclin D3 and MMP7 expression. *Int. J. Med. Sci.* **16**, 470–476
50. Behan, F. M., Iorio, F., Picco, G., Gonçalves, E., Beaver, C. M., Migliardi, G., Santos, R., Rao, Y., Sassi, F., Pinnelli, M., Ansari, R., Harper, S., Jackson, D. A., McRae, R., Pooley, R., Wilkinson, P., van der Meer, D., Dow, D., Buser-Doepner, C., Bertotti, A., Trusolino, L., Stronach, E. A., Saez-Rodriguez, J., Yusa, K., and Garnett, M. J. (2019) Prioritization of cancer therapeutic targets using CRISPR-Cas9 screens. [E-pub ahead of print] *Nature*
51. Remmerbach, T. W., Wottawah, F., Dietrich, J., Lincoln, B., Wittekind, C., and Guck, J. (2009) Oral cancer diagnosis by mechanical phenotyping. *Cancer Res.* **69**, 1728–1732
52. Lautenschläger, F., Paschke, S., Schinkinger, S., Bruel, A., Beil, M., and Guck, J. (2009) The regulatory role of cell mechanics for migration of differentiating myeloid cells. *Proc. Natl. Acad. Sci. USA* **106**, 15696–15701
53. Zheng, Y., Wen, J., Nguyen, J., Cachia, M. A., Wang, C., and Sun, Y. (2015) Decreased deformability of lymphocytes in chronic lymphocytic leukemia. *Sci. Rep.* **5**, 7613
54. Shibue, T., and Weinberg, R. A. (2017) EMT, CSCs, and drug resistance: the mechanistic link and clinical implications. *Nat. Rev. Clin. Oncol.* **14**, 611–629
55. Osanai, K., Kobayashi, Y., Otsu, M., Izawa, T., Sakai, K., and Iwashita, M. (2017) Ramelteon, a selective MT1/MT2 receptor agonist, suppresses the proliferation and invasiveness of endometrial cancer cells. *Hum. Cell* **30**, 209–215
56. Li, Y., Li, S., Zhou, Y., Meng, X., Zhang, J. J., Xu, D. P., and Li, H. B. (2017) Melatonin for the prevention and treatment of cancer. *Oncotarget* **8**, 39896–39921

Received for publication December 3, 2018.
Accepted for publication April 16, 2019.